Supporting information:

Dual-Modulation of Lysosomal Integrity via Alkalization and Lipid Peroxidation: A Promising Strategy for Tumor Inhibition

Donglin Liu[a,c,†], Jianzhi Mao[a,†], Yuying Dai[a], Kailin Li[a], Qiwei Tian[b,*], Fengfeng Xue[b], Shiping Yang[a,*], Lu An[a,*]

[a] *Shanghai Municipal Education Committee Key Laboratory of Molecular Imaging Probes and Sensors, Shanghai Normal University, Shanghai 200234, China*

[b] *Shanghai Key Laboratory of Molecular Imaging, Shanghai University of Medicine and Health Science, Shanghai 201318, China*

[c] *State Key Laboratory of Pharmaceutical Biotechnology, Division of Hepatobiliary and Transplantation Surgery, Department of General Surgery, Nanjing Drum Tower Hospital, The Affiliated Hospital of Nanjing University Medical School, Nanjing 210003, China*

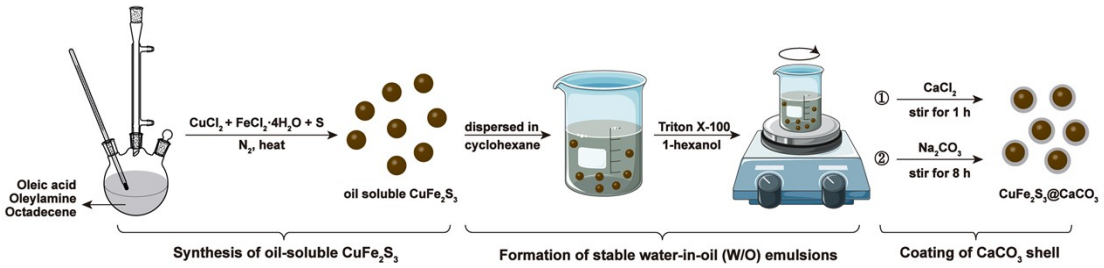

Fig. S1 Synthesis diagram of $CuFe_2S_3$@$CaCO_3$ nanocomposites.

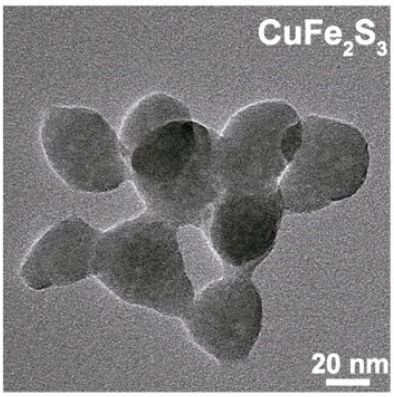

Fig. S2 TEM image of $CuFe_2S_3$ nanocomposites.

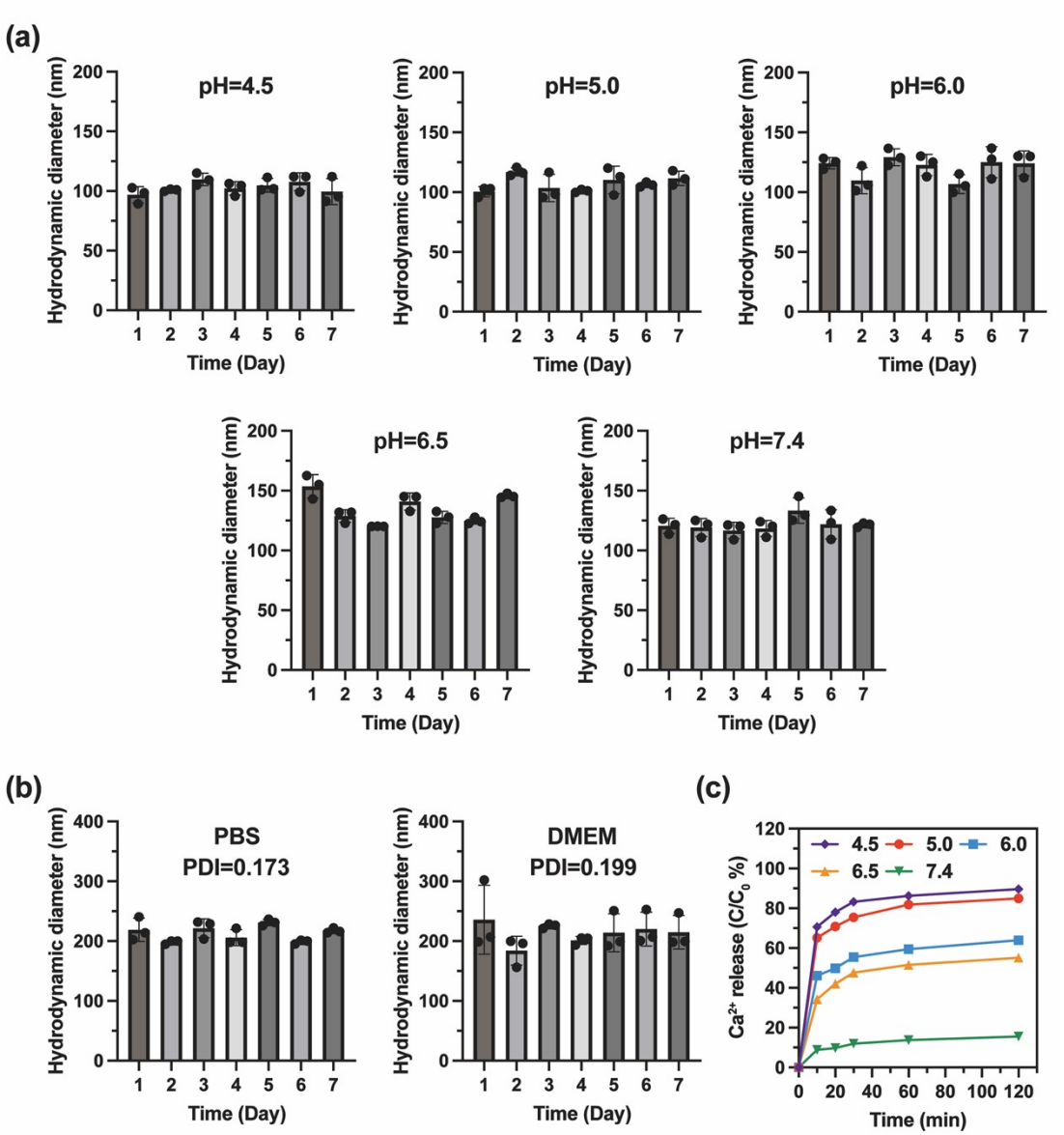

Fig. S3 (a) The particle size distribution of the $CuFe_2S_3$@$CaCO_3$ nanocomposites under different pH conditions. **(b)** The colloidal stability data and PDI values of $CuFe_2S_3$@$CaCO_3$ nanocomposites in physiological conditions. **(c)** Ca^{2+} release of $CuFe_2S_3$@$CaCO_3$ nanocomposites under different pH conditions.

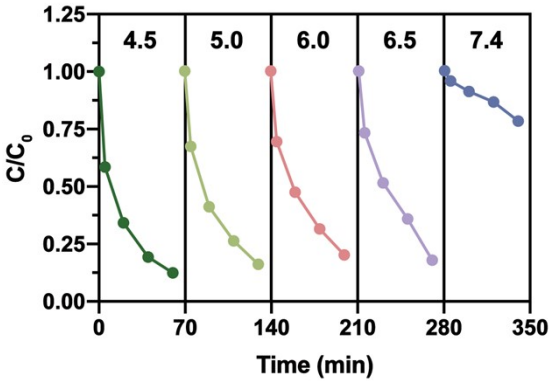

Fig. S4 Summary diagram of the degradation effect of $CuFe_2S_3$@$CaCO_3$ nanocomposites on MB under different pH values.

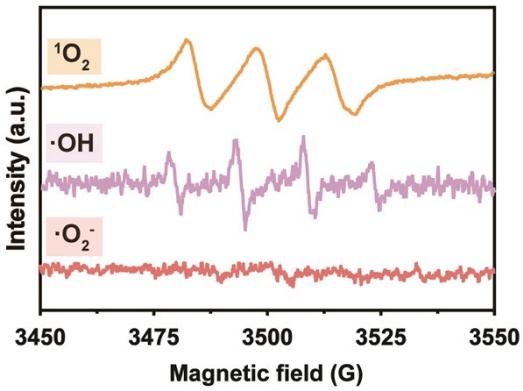

Fig. S5 EPR spectra of ROS generated by the $CuFe_2S_3$@$CaCO_3$ nanocomposites.

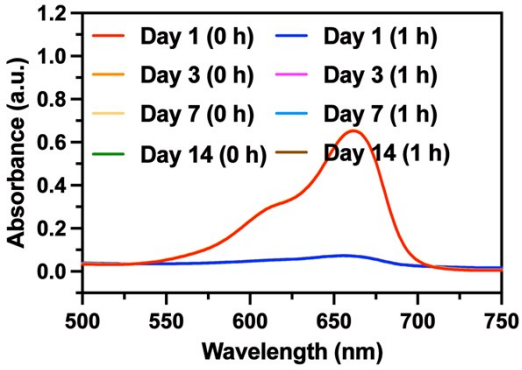

Fig. S6 ROS generation of $CuFe_2S_3$@$CaCO_3$ nanocomposites at days 1, 3, 7 and 14.

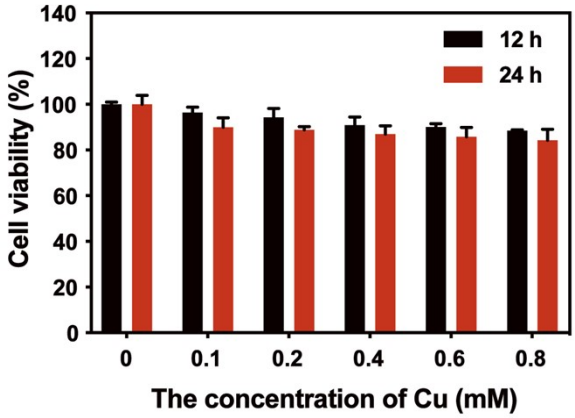

Fig. S7 Cytotoxicity of $CuFe_2S_3$@$CaCO_3$ nanocomposites to 4T1 cells.

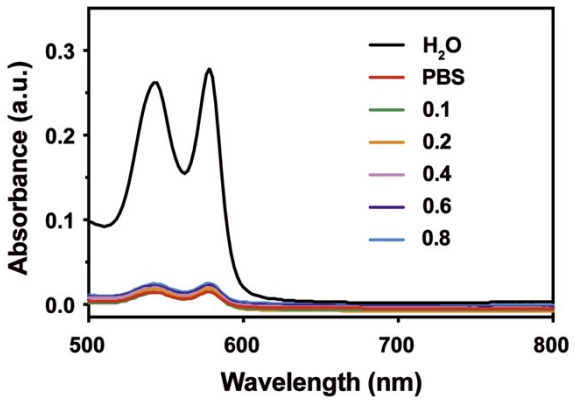

Fig. S8 Hemolytic absorption curve.

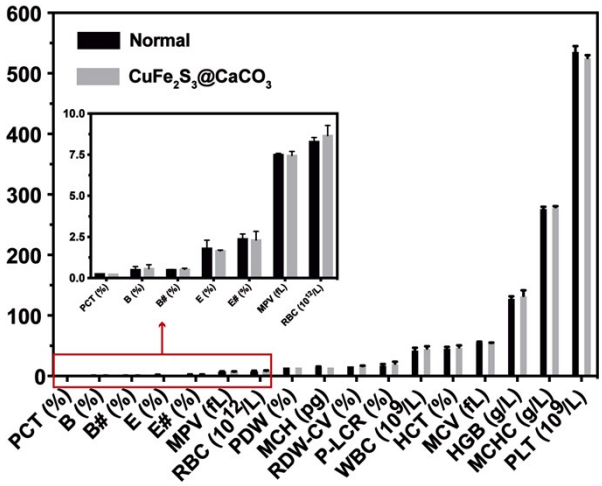

Fig. S9 Blood routine of mice before and after tail vein injection of $CuFe_2S_3$@$CaCO_3$ nanocomposites.

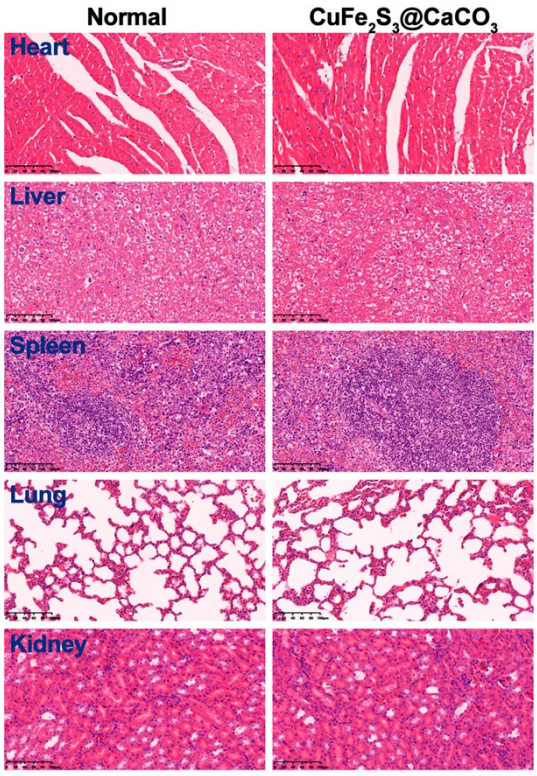

Fig. S10 H&E staining of heart, liver, spleen, lung and kidney sections from cured and normal mice (scale bar: 100 μm).

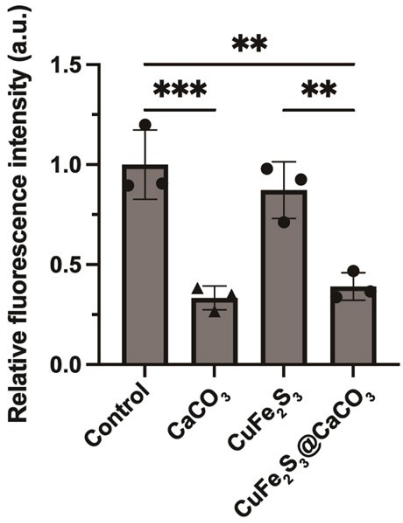

Fig. S11 Relative fluorescence intensity corresponding to P02 dye in Figure 4a (*p < 0.05, **p < 0.01, ***p < 0.001).

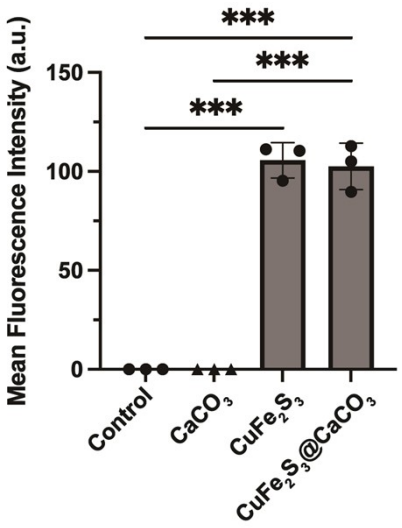

Fig. S12 Mean fluorescence intensity corresponding to DCFH-DA dye in Figure 4b (*p < 0.05, **p < 0.01, ***p < 0.001).

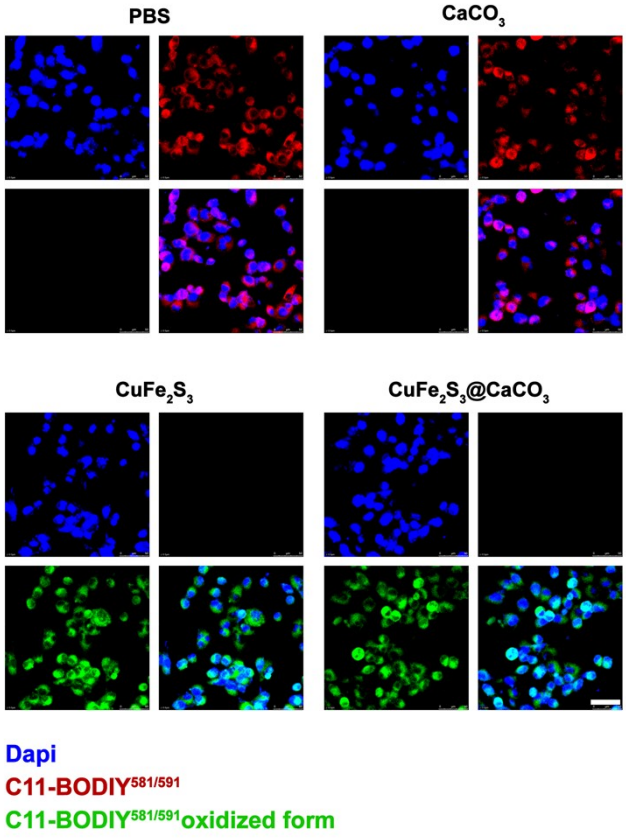

Fig. S13 CLSM images of 4T1 cells stained for lipid peroxidation after be treated in different groups (scale bar: 50 μm).

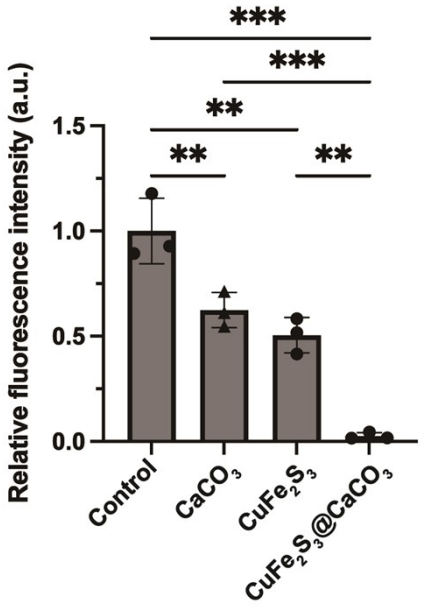

Fig. S14 Relative fluorescence intensity corresponding to AO (Red) dye in Figure 4b (*p < 0.05, **p < 0.01, ***p < 0.001).

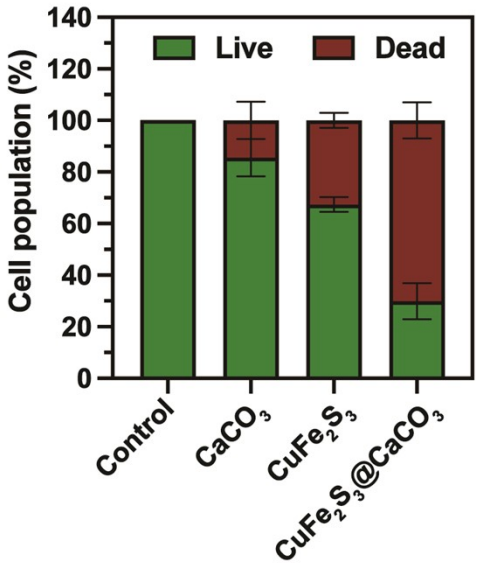

Fig. S15 Quantification of cell populations based on AM/PI staining.

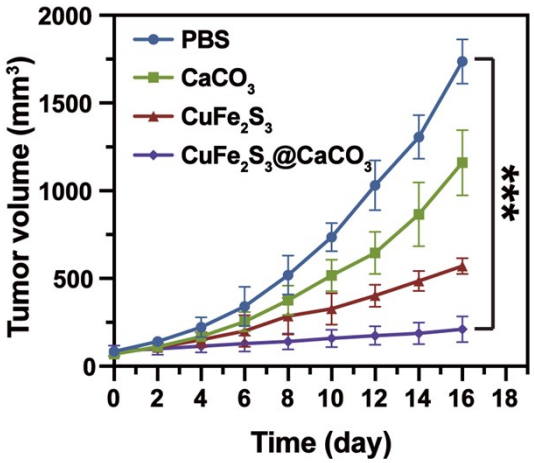

Fig. S16 Statistics of average tumor volume of mice in different treatment groups (*p < 0.05, **p < 0.01, ***p < 0.001).

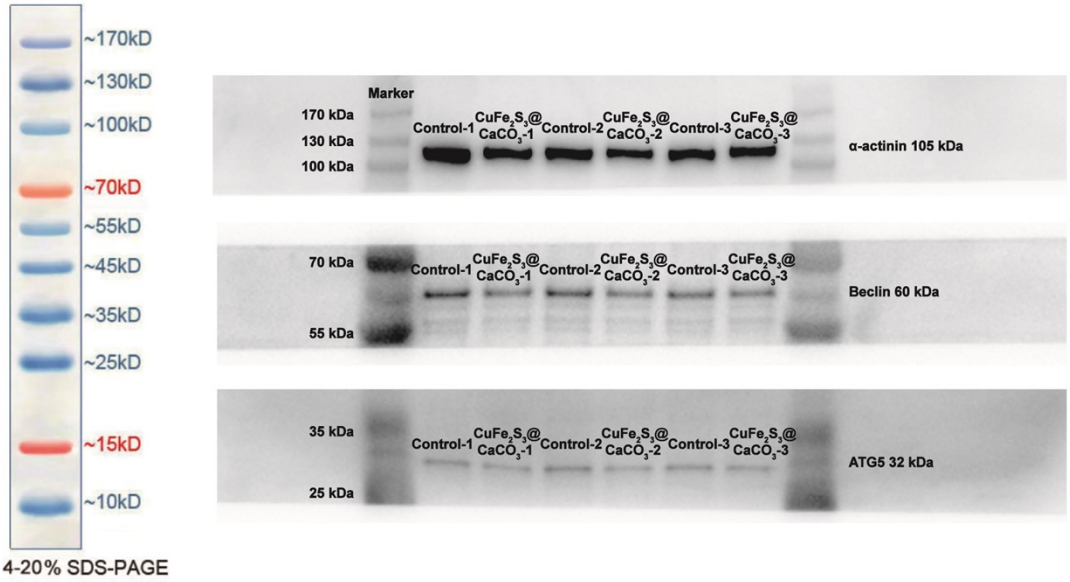

Fig. S17 The uncropped raw data of the Western blot corresponding to Figure 4f.